Comparison of different feedback controllers on an airfoil benchmark

Loïc Michel[1], Caroline Braud[2], Jean-Pierre Barbot[1,3], Franck Plestan[1], Dimitri Peaucelle[4], and Xavier Boucher[5]

[1]Nantes Université, Ecole Centrale Nantes, CNRS, LS2N, UMR 6004, 44000 Nantes, Nantes, France
[2]Nantes Université, Ecole Centrale Nantes, CNRS, LHEEA, UMR 6598, 44000 Nantes, Nantes, France
[3]ENSEA, Quartz Laboratory, EA 7393, 95014 Cergy-Pontoise, Cergy-Pontoise, France
[4]LAAS-CNRS, Université de Toulouse, CNRS, Toulouse, France
[5]Université du Québec à Trois-Rivières-LSSI, Trois-Rivières, Québec, Canada

Correspondence: Caroline Braud (caroline.braud@ec-nantes.fr)

Abstract. The present paper proposes a comparison of three well established controllers: a robust Proportional-Integral-Derivative (PID) controller (Conord and Peaucelle (2021)), a model-free control (Fliess and Join (2013, 2021)) and an adaptive sliding-mode control based on the super-twisting algorithm (Shtessel et al. (2023)). The benchmark considered is an airfoil section equipped with trailing edge jets, load sensors and a perturbation system. The objective is to track the lift command under external wind perturbations. Outcomes of this work are comparison of performances for three control laws that are suitable when little knowledge is known from the physics. This study not only quantifies performance in terms of load control, but also in the needed implementation effort.

1 Introduction

Controlling wind turbines is generally performed globally (rotor yaw or blade pitch control) to optimize the energy extraction or minimize rotor's loads for rotor's lifetime extension. This means that no information from the blade aerodynamics is up to now taken into account in the control loop while it is well understood that wind inflow interaction with blade aerodynamics can lead to power loss, load fluctuations and noise generation, see e.g. Wagner et al. (1996); Rezaeiha et al. (2017). Wind turbines are exposed to inflow turbulences of different scales due to the atmosphere in which they operate (see e.g. Schepers et al. (2021)) and also to rotor misalignment with the inflow or wakes of neighboring turbines. This is even more significant for offshore wind turbines whose rotor diameter are significantly larger, with local shear inflow over the rotor sweep area and even along the blades. To alleviate loads, the pitch control Bossanyi (2000) can be complemented by local and sometimes faster aerodynamic controllers. Local actuator types (such as vortex generators, flaps, slats, micro-jets / plasma) and sensor types (e.g. e-penons) have been developed for that purpose. Few contributions of control algorithms sufficiently robust to operate on the wind turbine blade aerodynamics have been proposed so far. Particularly, a significant number of controllers were investigated for NACA profiles with objectives towards aeronautic applications, see e.g. Becker et al. (2007). More recently, different control technologies for wind energy applications were reviewed in Aubrun et al. (2017). Along with the development

of AFC devices and open-loop tests came the development of closed-loop tests using advanced controllers with the early work of Allan et al. (2000) using a model-based approach. A comprehensive review of control strategies dedicated to gust alleviation problems using active flow control is presented in Williams and King (2018). Feedback and feed-forward structures based on system identification have been investigated for active load reduction in the context of a controlled wind turbine blade (see e.g. Becker et al. (2005); Barlas et al. (2008); Li and Balas (2013); Jaunet and Braud (2018); Peaucelle et al. (2019); Bartholomay et al. (2021)). At last, some model-free approaches were explored for load alleviation objective in Becker et al. (2005), Michel et al. (2022) or Michel et al. (2024) based on different the well established modeling techniques from respectivelly Scheinker (2024); Fliess and Join (2021); Shtessel et al. (2023).

However, none of the control algorithms were compared on the same airfoil benchmark. It is well-known that airfoils exhibit very different phenomena due to different shapes, Reynolds numbers etc. (see e.g. McCullough and Gault (1951),Gault (1957)) that are still investigated (see e.g. Brunner et al. (2021), Braud et al. (2024)). In the present work different control strategies, model-based and model-free types, were investigated on the same airfoil configuration which serves as a benchmark to highlight pros and cons with respect to different criteria.

The purpose of this study is to evaluate the performances of some selected feedback control strategies under different operating conditions of an experimental airfoil bench. The main goal is to alleviate aerodynamic load fluctuations and is tested with respect to large mean flow variations with turbulence superposed to it. The experimental setup is by itself a contribution as it can serve in the future to test more control laws in different configurations which are both simple and realistic compared to industrial applications. The second, yet main contribution, is to design and test three types of controls: the robust. The tests allow the characterization of operating domains for each control law regarding criteria like the nominal lift responses, the rejection of high frequency fluctuations, and the robustness with respect to modifications on the dynamics due to changes of the air flow characteristics. The outcome of the study is a comprehensive exposure of the pros and cons of each feedback control approach, not only for the produced performances for the load control itself, but also in terms of needed efforts for the design and the implementation of these controls.

In this work, three control laws are being investigated. They have been chosen based on the experience of the automatic control collaborators of this study and, rather than investigating all possible solution at their hand, we specifically selected those control strategies that are suitable for cases where there is little precise knowledge on the system to control and limited algorithmic complexity on implementation level. The three control laws are: (a) a robust Proportional-Integral-Derivative (PID) controller (Conord and Peaucelle (2021)) which has the simplicity of the classical basic PID while providing potentially robustness and close to equilibrium perturbation rejection performances; (b) a model-free control (Fliess and Join (2013, 2021)) which requires little online tuning; (c) an adaptive sliding-mode control based on the super-twisting algorithm (Shtessel et al. (2023)) which also requires little knowledge about the model and has interesting finite-time convergence properties.

The paper is structured as follow. Section 2 presents the experimental setup. Section 3 presents the control problem and the control strategies that will be exploited. Section 4 discusses the results and Section 5 gives some concluding remarks.

2 Experimental setup

The main purpose of this experiment is to highlight the feasibility of using advanced control algorithms within a simplified flow configuration. Simplifications stand in the Reynolds number, the blade shape and the 2D section (no rotation and no transverse flow). This means that the flow characteristics (location of flow transition from laminar to turbulent, location of flow separation and thus aerodynamic loads) may differ from real applications. However, we show that even with such basic assumptions, the feedback control of the lift is possible and has sufficient robustness for potential usage in more realistic situations beyond 2D blade section assumptions.

In order to be self-content, we recall that the experimental closed-loop bench already presented in Michel et al. (2024) (see Figure 1 for pictures and Figure 2 for a functional scheme) is composed of a wind tunnel with its perturbation system (gust generator), a 2D aerodynamic blade profile equipped by micro-jets and load sensors to measure lift and drag.

(a) Blade and its instrumentation & micro-jet system   (b) Chopper rotor in the wind tunnel
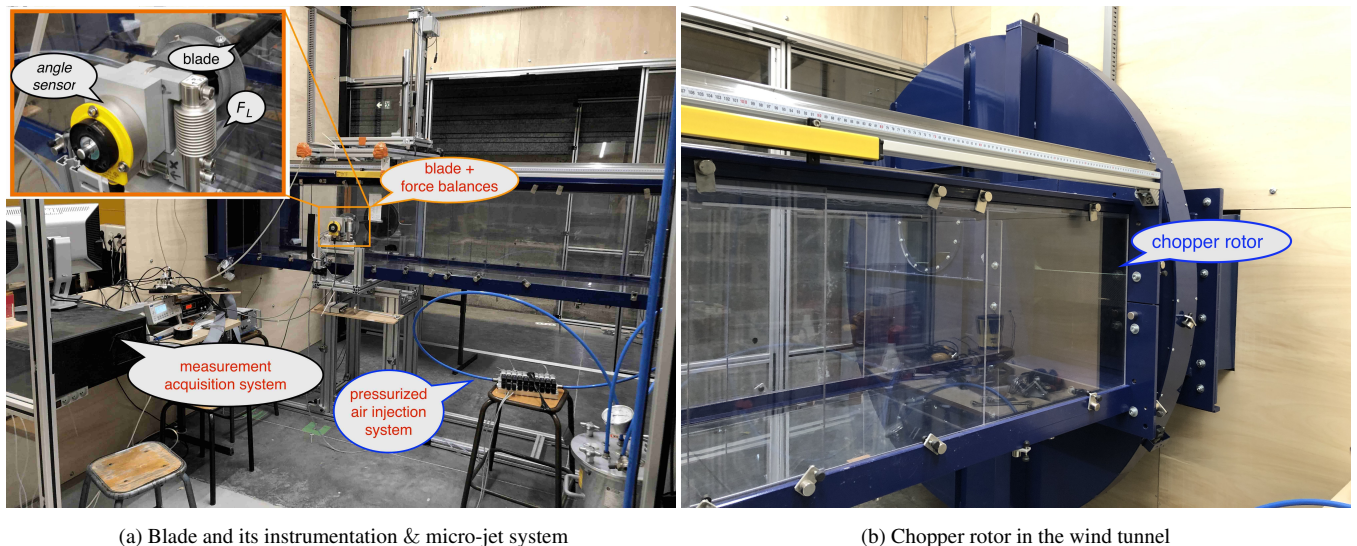
Figure 1. The wind tunnel test bench composed of: a) the test section with all needed instrumentation (blade, load measurement system, angle sensor, acquisition and actuation systems) and b) the perturbation system, also called the chopper (see Neunaber and Braud (2020)). The actuation system is made of pressurized air circuit (blue tubes) that are connected to a first reservoir in the bottom right of the image and to the solenoid valves set on the stool. Two vinyl tubes are connecting from the exit of two solenoid valves to the ends of the hollow tube inside the blade. Extracted from Michel et al. (2024).

2.1 Wind tunnel facility and gust generator

The LHEEA aerodynamic wind tunnel is a recirculating one. The test section has a cross-section of $500 \times 500 \mathrm{mm}^2$ and a length of $2300 \mathrm{\,mm}$ (Figure 2). The turbulence intensity of an undisturbed inflow in the wind tunnel is around 0.3%. In the present study, a grid is installed at the inlet of the test section to generate turbulent inflow with a turbulence intensity of 3%. This
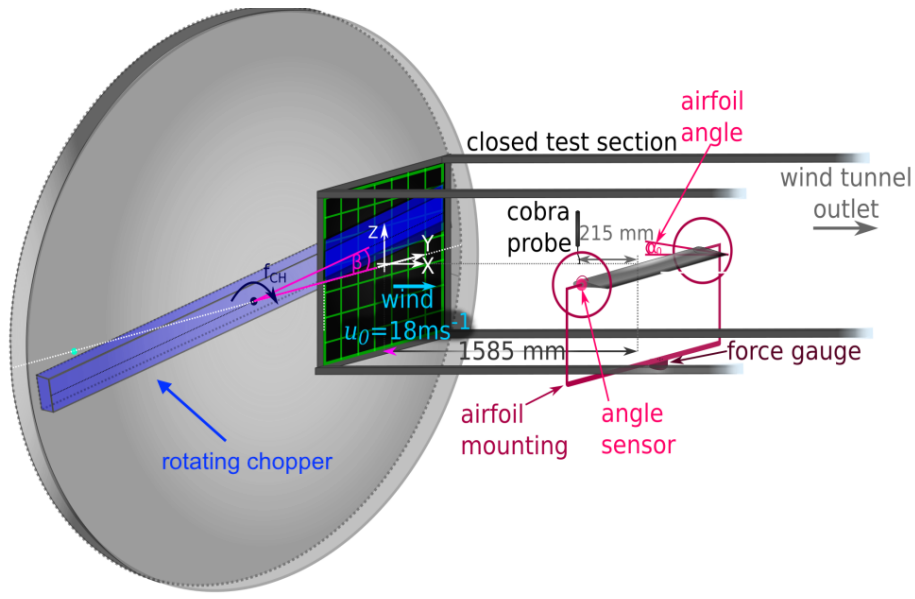
Figure 2. Scheme of the wind tunnel test bench including the chopper and the uniform grid, the mounted airfoil, the angle sensor and the force gauge (load sensor). Extracted from Michel et al. (2024).
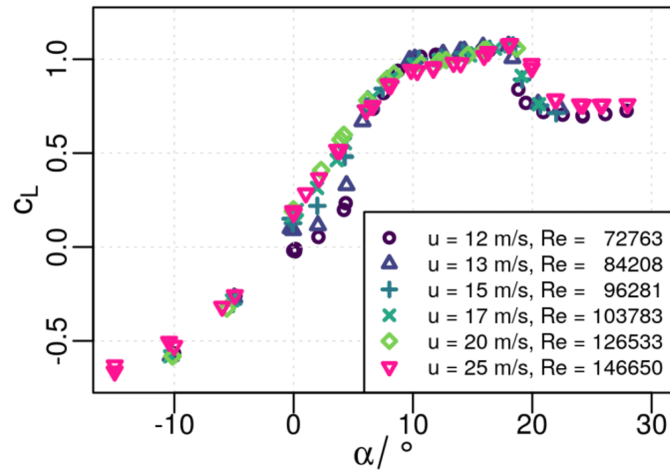
Figure 3. Reynolds number effect on the lift coefficient curve, C_L versus the angle of attack α. Extracted from Michel et al. (2024).

bypasses the laminar-to-turbulent transition occurring at low Reynolds numbers and low angles of attack (AoA) with respect to this blade geometry (see the linear part of the lift curve in Figure 3).

The inlet of the test section is additionally equipped with a system which enables the generation of a sudden variation of the mean flow with turbulence superimposed on it (for more details see Neunaber and Braud (2020)). This system is called "chopper" and consists of a rotating bar that cuts through the inlet of the test section (Figure 2).

2.2 Aerodynamic profile

A 2D blade section of type NACA $65_4 - 421$ with a chord length of $c = 9.6\,\mathrm{cm}$ is installed in the test section of the wind tunnel[1]. It is a thick profile with two changes of the lift curve corresponding to a first boundary layer separation at the trailing edge of the profile and a second flow separation at the leading edge, indicating stall (see Soulier et al. (2021) for more details on the blade aerodynamics). In the present study, the angle of incidence is set to $\alpha = 20°$ that corresponds to the maximum of increase of the lift (see. Fig. 3) considering the additional micro-jet [2]. More investigations are needed to extend the present work to other angles of incidence.

2.3 Micro-jets

To control the flow around the airfoil, holes of $1\,\mathrm{mm}$ diameter with equidistant $8\,\mathrm{mm}$ spacing are placed at $1.92\,\mathrm{cm}$ from the airfoil's trailing edge, along the entire spanwise direction (Figure 4). They are connected to a plenum chamber, itself fed with pressurized air at 6 bars. The plenum chamber is an hollow tube placed along and inside the blade, in the spanwise direction, tangent to the airfoil surface, with holes on it. Jets are coming out of these holes when hollow tube ends are connected to the air circuit. This prevents the individual control of jets, however, this ensures the jet amplitude homogeneity in the spanwise direction. The air circuit is connected to solenoid valves that switch On/Off simultaneously, using a single control law so that synchronous pulsed micro-jets can be generated with a repetition rate of up to $300\,\mathrm{Hz}$.

The action of the micro-jets is physically limited to the injection of pressurized air of maximum 6 bars, thus defining the range of the lift variations that can be compensated by the micro-jets actuator system. It is identified by a simple succession of valves opening and closing.

2.4 Lift and drag measurements

Two Z6FC3 HBM bending beam load cell sensors were used on each side of the blade support to measure the lift (Y_1, Y_2) and drag forces (X_1, X_2). They were calibrated *in situ* using calibrated weights from $0 - 5\,\mathrm{kg}$ in steps of $0.5\,\mathrm{kg}$.

---

[1]Note that "2D blade section" here refers to a two-dimensional shape that is extruded in the third dimension so that the blade section spans the whole length of the wind tunnel.

[2]Some additional open-loop tests for $\alpha = \{0°, 10°, 20°\}$ have been performed to chose this value (see *e.g.* the Fig. 4 in Michel et al. (2024)). It has been shown that only a low range of the lift variation (or controlability margin of the lift) can be reached for $\alpha = 0°$ when the flow is still attached (*i.e.* maximum lift force gain $\Delta F_L = 2.5\,\mathrm{N}$). At $\alpha = 10°$, the controlability margin is three times higher ($\Delta F_L = 7\,\mathrm{N}$), but it is decreasing with the inlet pressure from $p = 1$ bar. An angle $\alpha = 20°$ is therefore chosen to operate the control algorithm, as the controlability margin is higher and linearly increasing according to the inlet pressure.

 ## 2.5   Control hardware

The control is managed by a STM32 Nucleo board H743ZI2 allowing a 16-bit ADC acquisition as well as the possibility to monitor the signals in real-time on the computer. The lift force is measured by the force balances (Y_1, Y_2) and is acquired at a sampling rate of $20\,\text{kHz}$ using the Nucleo board. The signal is filtered using a fourth order Butterworth filter with a cut-off frequency of $20\,\text{Hz}$. The control updates at $20\,\text{kHz}$ and drives the valve at $200\,\text{Hz}$ in response to the input from the force
100   balances.

3   Control methodology

In this section, the control problem is presented with respect to the leak of aerodynamic modeling well adapted to the control design.

3.1   Problem statement

105   All along the paper, the control of the lift is performed by a control loop that drives the pressurized air towards holes on the blade surface (Fig. 4), named micro-jets, which modifies the local pressure (that induces the lift), to track the lift reference. Since we use a small scale of the blade (1/10), all the holes are driven by a single control law, assuming that the wind profile is equally distributed along the considered section of the blade under study.
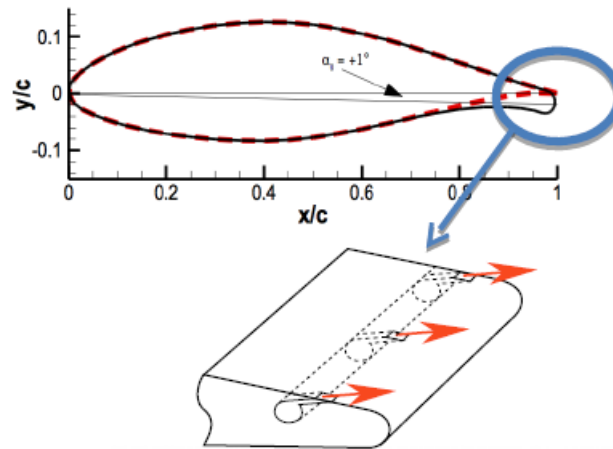
Figure 4. Mechanical configuration of micro-jets on the blade section. Extracted from Michel et al. (2024)

In the sequel, the control input of the system is denoted u, and the output that is controlled, denoted y, is the lift force.
110   Considering the lift reference y^*, the goal of the closed-loop control is to ensure that the measured lift y converges with "accuracy" to y^*.

The purpose of the study is to perform comparisons between controllers in order to evaluate performances such as time-response, tracking precision, delay to desaturate, taking into account the properties and the practical implementation of each controller, regarding several operating conditions of the lift control system.

3.1.1 PID Robust Control (PID)

The lift variation in response to micro-jet actuation can be modelled as a second order system in first approximation (see Brunton and Rowley (2010)). Such approximate model is highly dependent of particular aerodynamic operating condition, including specific inflow velocity, pitch, etc. One way to cope with several operating points as a whole is to consider such second order models with uncertain parameters. A rather simple way to build uncertain models can be achieved by considering a finite set of relevant operating points at which specific models are identified, assuming that the true parameters to be in the convex set of the parameters obtained at these relevant operating points. Such modeling is known as polytopic modeling where state-space matrices can take infinitely many possible values within the set composed of all convex combinations of finitely many vertices. Robust control aims at assessing stability (and other performances) for all possible realisation of the system in the polytope. Robust evaluations of performances are necessarily pessimistic compared to the true performance of the system at one specific operating condition. On the other hand, it gives guarantees of stability and other performances, at least, as long as the modeling assumptions hold true.

In this paper, we used control design results from Conord and Peaucelle (2021) that are implemented in the R-Romuloc toolbox Peaucelle et al. (2014). These results allow the design of state-feedback controllers. They rely on Lyapunov-type methods and solve the design problem based on linear matrix inequality formulas solved by semi-definite programming tools. We identified state-space representation in controllable canonical form where the states are the error $e = y^* - y$ between the reference y^* and the true lift measure y, and the time-derivative of this error. An artificial state as the integral of the error is added, hence, the state-space design provides exactly a PID controller of the type:

$$u = K_\mathrm{p}e + K_\mathrm{i} \int_0^t e(\tau)\,\mathrm{d}\tau + K_\mathrm{d}\dot{e} \tag{1}$$

where $K_\mathrm{p}, K_\mathrm{i}, K_\mathrm{d}$ are designed gains.

In order to evaluate the influence of the identified models on the performances of the closed-loop system, we performed the design procedure for three different choices of polytopes. The design is systematic assuming the learning of appropriate second order models is done and does not rely on tuning skills of some smart operator. The more operating points are considered, the more robust the controller shall be. Due to the upper defined pessimism, it may also have poor performance at specific operating conditions. Poor performance can also come from discrepancies between true dynamics (which are not linear of order two) and the identified models.

3.1.2 Model-Free Control (MFC)

Full details on model-free control are given in Fliess and Join (2013). Its usefulness in many situations, including compensating severe non-linearities and time-varying reference signals, has been demonstrated (see *e.g.* Lafont et al. (2020) Park et al. (2021)). The corresponding intelligent controllers are much easier to implement and to tune than standard PID controllers which are today the main tool in industrial control engineering (see, e.g., Åström and Murray (2008)).

The ultra-local model

In the current application, the unknown description of the plant is restricted to a SISO (single-input single-output) system because the objective is to control only the lift y (output) using the actuator u (input). The unknown description of the SISO plant is replaced by an ultra-local first order model (*i.e.* that approximates very locally the overall dynamics of the system, see Fliess and Join (2013))

$$\dot{e} = \dot{y}^* - \dot{y} = \dot{y}^* - (F + \beta u) \tag{2}$$

where: the control and output variables are respectively u and y; the time-varying quantity F is estimated online and subsumes the unknown internal structure and the external disturbances. The constant $\beta \in \mathbb{R}$ is chosen by the practitioner such that $\dot{y}$ and βu are of the same magnitude. Therefore, β does not need to be precisely estimated.

Equation (2) is only valid during a short time lapse that must be continuously updated: it implies that F is estimated on-line through the knowledge of the control output u and the numerical differentiation of y. It is natural to consider firstly the ultra-local model (2) of the first order, for which, in the considered case, experimental results show that this particular order of the F model gives results that are accurate enough regarding the present objective of the paper (track lift reference).

Intelligent P controllers

The control law reads as the *intelligent P controller*, or *i-P* controller

$$u = -\frac{F - \dot{y}^*}{\beta} + K_{\mathrm{p}} e \tag{3}$$

where β is a parameter and K_{p} is the usual tuning gain that have to be set by the user.

The i-P controller (3) is compensating the poorly known term F. Controlling the system therefore boils down to the control of an elementary pure integrator. To numerically estimate the derivative of y, homogeneous semi-implicit differentiators have been used (see Michel et al. (2021); Mojallizadeh et al. (2023)) .

3.1.3 Adaptive Super Twisting control (AST)

Full details on adaptive super-twisting can be found in Mirzaei et al. (2022). The dynamics of the tracking error is assumed to be given by

$$\dot{e} = a + b u, \quad b \neq 0, \tag{4}$$

where a and b are unknown terms that are bounded in the operational domain; following the gained experience with MFC, it assumes that the relative degree[3] is equal to one. The objective in this work is to leverage the properties of the adaptive super-twisting algorithm as a model-free control law, *i.e.*, without any knowledge of a and b. From Plestan and Taleb (2021), the adaptive super-twisting controller is defined as

$$u = -k_1 |e|^{\frac{1}{2}} \operatorname{sgn}(e) + v$$
$$\dot{v} = -k_2 \operatorname{sgn}(e)$$

including the adaptive rules for the gains k_1 and k_2

$$\dot{k_1} = \begin{cases} \frac{\mu}{|\psi| + \epsilon_0} & \text{if} \quad |e| > \epsilon_0 \\ -k_1 & \text{if} \quad |e| \le \epsilon_0 \end{cases} \quad ; \dot{k_2} = \begin{cases} \frac{\mu}{2|e|^{\frac{1}{2}}} & \text{if} \quad |e| > \epsilon_0 \\ -k_2 & \text{if} \quad |e| \le \epsilon_0 \end{cases}$$

where $\psi = -\hat{\dot{e}}, \quad \mu = \mu_0 \left(|k_1| \sqrt{|e|} + |\psi| + \int_0^t k_2 \operatorname{sgn}(e(\tau)) d\tau \right), \quad (\epsilon_0, \mu_0) > 0$

and $\hat{\dot{e}}$ is the numerical estimation of $\dot{e}$. The main advantages of the AST controller are:

– the adaptive algorithm requires only limited information about the system modeling;

– the adaptive algorithm is well-known for its robustness;

– the adaptation of gains k_1 and k_2 helps reducing input energy consumption.

Note that these two approaches have different principles: the MFC can be considered as an extended classical control, based on an internal estimation of a ultra-local model, that approximates on-line the dynamic of the controlled system, whereas the AST is a high order sliding mode controller, whose gains are auto-adapted on-line and has conceptually a finite time convergence instead of an asymptotic convergence for all other tested control laws.

Figure 5 depicts the corresponding closed-loop of the proposed control architecture including the wind and chopper perturbations.

3.2 Control law improvement

To deal with the physical limits of the micro-jet actuator, that may create uncontrollable situations and unexpected behavior of the control algorithm in presence of strong perturbations of the lift, an anti-windup procedure from Tarbouriech et al. (2011) is proposed to manage the integration part of the robust PID controller and the adaptive super-twisting algorithm when physical saturation occurs. In this study, only upper saturation is in effect due to the choice of particular experiment tests. Nevertheless, the actuator has upper and lower limitations due to the physical limitations of the experimental test-bench.

---

[3]The relative degree corresponds to the minimum differentiability of the output y before seeing the input u (see Isidori (1985)).

3.2.1 Discretization of the control

To implement the control laws into the STM board, discretized versions have been derived from the continuous versions presented in the previous section. Every control laws are "sampled" under basic Euler discretization strategies regarding the integrators parts: PID contains a single integrator and AST contains four integrators; these integrators were solved using for example a numerical trapezoidal rule. However, contrarily to the PID (1), the MFC ultra-local model structure (2) does not contain integrators. Consequently, the sole discretization problem refers to the numerical time-derivative.
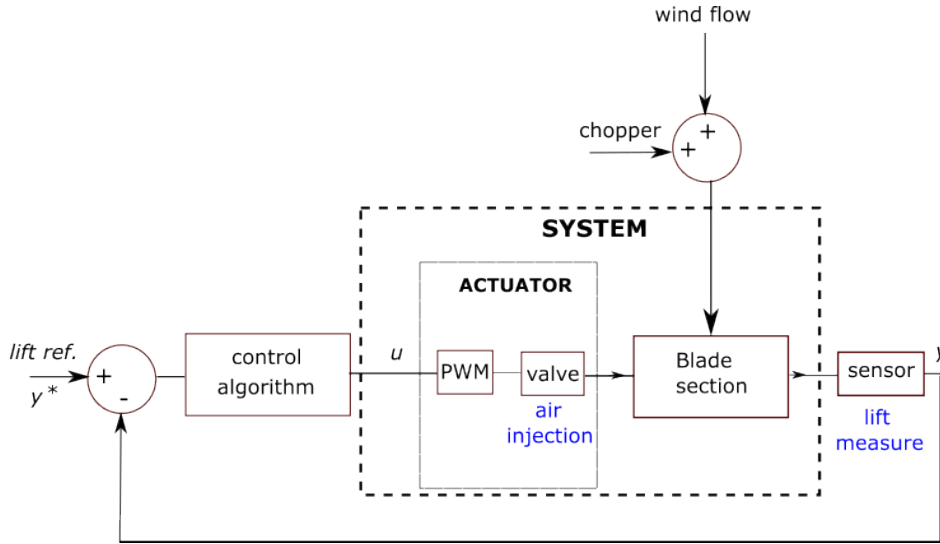
Figure 5. Closed-loop scheme: the system is made of a plant - the blade section, an actuator - the solenoid valves connected to compressed air and driven simultaneously by a PWM command, a perturbation from variation of the mean flow and the chopper system, a control algorithm and a lift sensor, which value is compared to the lift reference value and fed back to the control algorithm.

Due to the binary nature of the solenoid valves, the "continuous evolution" of the control output is converted into variations of the duty-cycle signal of a square signal that drives the valves; the period of the Pulse-Width Modulation (PWM) is set to $T_c = 200$ Hz. The quantification of the duty-cycle is a very important issue that may affect the quality of the tracking, even the stability of the overall control. Although the control algorithms provide "continuous" values, the conversion into the duty-cycle format requires to quantify the values of the control output since the practical implementation of the duty-cycle is incremental: in particular, the pressure of 6 bars has been "swept" under a precision of 4000 points, meaning that the error of quantification of the pressure injected to the valve actuator is about 1.5×10^{-3} bars. A high error of quantification gives less output resolution for the control to drive the pressure inducing strong oscillations of the measured lift. The choice of the precision is a compromise between 'minimal' tracking performances of the lift and the capabilities of the STM board (related to the maximum clock frequency) to increase the incremental precision of the duty-cycle since the control algorithm is updated at 20 kHz.

3.2.2 Definition of the saturation

The control is designed with respect to the saturation / physical limitation of the micro-jet actuator including a hysteresis and an anti-windup algorithm that interact with the numerical integration schemes of the controller.

Due to the physical limitation of the actuator, the output of the control is blocked / bounded when the control attempts to drive the lift outside the physical range of the admissible pressure of the valve actuator. The purpose of the anti-windup (AW) algorithm is complementary to the control blocking and holds the value of the control by freezing the integration part of the control algorithms to prevent from divergence or unexpected issue of the control. The anti-windup is tested in this work by considering the starting of the lift reference greater than the physical allowed pressure.

- In the PID case, the simplest solution is to freeze the integrator part during the saturation time.

- In the AST case, the simplest solution is also to freeze all the integrators during the saturation time, and especially the integration of the adaptive gains k_1 and k_2 since such adaptation is totally wrong while saturating.

- In the MFC case, blocking on the control law, the output of the control using a simple saturation is a solution to maintain the "learning effect" of the control and satisfy the input constraints.

4 Experimental results

4.1 Practical implementation

The model-free based approaches (MFC and AST) require few information, like the relative degree and the sign of gain of the system. Regarding the robust PID control, it requires a transfer function modeling at some specifically operating points.

- A robust PID controller is typically the simplest controller to implement within an embedded calculator and it can give excellent results for an 'unknown' dynamics, based on very rough modeling, but it is also very sensitive to changes and error of the modeling, which make the solution not efficient for a such application, as the unsteady aerodynamics on wind turbine blades may vary significantly with atmospheric conditions. The recent advances in robust control design allows building a robust control based on rough polytopic modeling. This polytopic modeling induces also some implicit assumption with respect to the model validity domain with regards to our application. Three polytopic models have been considered from different operating conditions (inflow velocity variations and different blockage ratios), in order to synthesize three PID controller, whose robustness has been tested separately towards the different proposed modeling. This approach requires an identification procedure to build the polytopes and the resulting synthesis of the robust control has been made using a dedicated Matlab® toolbox. The more precise the polytopic approximation, the more effective the control, but this will require a lot of time and effort.

- The MFC is of the same complexity as the PID, including a prediction part that requires the estimation of a numerical time-derivative of y.

– The AST contains several integrators that manage the dynamic of the internal integrator and the dynamic of the gains.

Both model-free solutions are of interest because they do not need any prior modeling of the system making these solutions pretty well adapted to control fluid dynamics applications. The tuning of the MFC and AST has been made according to the gained experience from Michel et al. (2022, 2024) and is consequently faster compared to the PID robust design (which requires a complete identification procedure (see *e.g* Albertos and Sala (2002)).

4.2 Scenarios of operation

Several cases of operating conditions have been considered to compare model-based approach (robust PID control) and model-free based approach (MFC and AST) in terms of usual performances: the sum of square error (SSE) representing the energy of the control signal, $\mathrm{SSE} = \sum_k (e_k)^2$, the variation of the control input (VarU), $\mathrm{VarU} = \sum_k |u_{k+1} - u_k|$ and the usual standard deviation of the ouput y, $\mathrm{STD} = \sqrt{Variance(y)}$, as well as the time responses and the desaturation time.

The efficiency of the lift tracking is evaluated for several scenarios that illustrate different operating conditions, defined by different inflow velocities and different fixed positions of the chopper in the test section, for which the characteristics are described below and are summarized in the Table 1. The chopper induces different perturbation levels defined as the ratio in percentage $S_p = \frac{S_{bar}}{S} \times 100$, with S_{bar} the chopper surface area introduced in the test section and S the surface area of the test section such as $S_p = \{0, 0.6, 2.5\}\%$. Due to the difference of dynamic between the chopper displacement and aerodynamic phenomena including the micro-jet feedback loop, in this paper, the chopper is maintained at a fixed position for which its displacement is considered as instantaneous.

The experiments are conducted considering a constant inflow velocity of $20\,\mathrm{m.s}^{-1}$, except for the scenario 1 which considers an inflow velocity of $19\,\mathrm{m.s}^{-1}$, measured with a Pitot tube in front of the airfoil in the undisturbed flow (before the chopper), and an angle of attack of the 2D blade section of $20°$. The tracking lift reference starts with a half sine that aims to provide some dynamics to initiate the control, and then, the reference is composed of several constant piecewise parts to induce small variations of the controlled lift. The chopper, when introduced slightly in the test section, reduces the mean inflow velocity and adds turbulence. The chopper is used to evaluate the robustness of the controllers under perturbations of the lift and quantified using the ratio between the chopper surface area and the test section area as introduced in the previous Section 2.1. reported in percentage, it represents the blockage coefficient created by the chopper; the time duration during which the chopper is introduced in the test section is indicated together with the blockage coefficient in Tab 1.

Scenario 1: This starting scenario considers the simplest case where the inflow velocity is set to a constant low value of $19\,\mathrm{m.s}^{-1}$ and no perturbation is introduced.

Scenario 2: The inflow velocity is set to $20\,\mathrm{m.s}^{-1}$ and the chopper is manually introduced at $t < 10$ s to disturb the air flow (fixed at $0.6\,\%$).

Scenario 3: The inflow velocity is set to $20\,\mathrm{m.s}^{-1}$ and the chopper is manually introduced at $t < 10$ s to disturb the air flow (fixed at $2.5\,\%$).

Scenario 4: The inflow velocity is set to $20\,\text{m.s}^{-1}$, then changed to $21\,\text{m.s}^{-1}$ at $t = 10$ s. The chopper is manually introduced at the beginning to disturb the air flow (fixed at 0.6 %).

Scenario 5: The inflow velocity is set to $20\,\text{m.s}^{-1}$, then changed to $21\,\text{m.s}^{-1}$ at $t = 10$ s. The chopper is manually introduced at the beginning to disturb the air flow (fixed at 2.5 %).

Scenario 6: The inflow velocity is set to $20\,\text{m.s}^{-1}$. The chopper is introduced between $t = 10$ s and $t = 60$ s to disturb the air flow (fixed at 2.5 %).

To illustrate the operation of the saturation mode, a higher output reference than the maximum reachable lift is firstly considered in order to saturate the micro-jet actuator, then a piece-wise constant reference is applied to track the lift.

Sc. #	Inflow velocity	Blockage ratio
1	$19\,\text{m.s}^{-1}$ constant	–
2	$20\,\text{m.s}^{-1}$ constant	0.6 % starting $t < 10$ sec
3	$20\,\text{m.s}^{-1}$ constant	2.5 % starting $t < 10$ sec
4	$20\,\text{m.s}^{-1}$ then $21\,\text{m.s}^{-1}$ starting at 30 sec	0.6 % starting at the beginning
5	$20\,\text{m.s}^{-1}$ then $21\,\text{m.s}^{-1}$ starting at 30 sec	2.5 % starting at the beginning
6	$20\,\text{m.s}^{-1}$ constant	2.5 % over $10 < t < 60$ sec

Table 1. Overview of scenarios of operation.

4.3 Setup of the controllers

Table 2 summarizes parameters of controller that have been used for each scenario. In particular, concerning the PID control, the (a), (b) and (c) controllers have been synthesized based on three polytopes that combine several operating conditions, that are summarized in Table 3.

type	K_{p}	β	ϵ_0	μ_0	PID_{Kd}	PID_{Ki}	PID_{Kp}
MFC	0.0002	0.0002					
AST			20	1.5			
PID(a)					1.37×10^{-6}	2.498	1.96×10^{-4}
PID(b)					-1.3×10^{-7}	5.675	1.906×10^{-4}
PID(c)					-2.4×10^{-7}	5.975	1.901×10^{-4}

Table 2. Parameters of the controllers

Remark that, if one adds to the polytope (a) the model identified for 2.5 % for the inflow velocity of $21.3\,\text{m.s}^{-1}$ the R-Romuloc toolbox fails to find a solution. This could be either because of the conservativeness of the coded method or because no such robust PID exists.

	inflow velocity 19 m.s^{-1}			inflow velocity 20 m.s^{-1}			inflow velocity 21 m.s^{-1}		
polytope	0 %	0.6 %	2.5 %	0 %	0.6 %	2.5 %	0 %	0.6 %	2.5 %
(a) 8 matrices	X	X	X	X	X	X	X	X	
(b) 3 matrices	X	X	X						
(c) 3 matrices		X		X		X			

Table 3. Polytope definitions of the PID controllers.

4.4 Results and discussion

290 In this section, the experimental results are presented considering firstly no actuator saturation during the lift tracking, and then, with actuator saturation.

4.4.1 Analysis of performances in case of no control saturation

Throughout this sub-section, it has been verified that the measured lift does not saturate, meaning, that the evolution of the input u is not limited by the AW algorithm.

295 The performances of the controllers with respect to the tracking error are evaluated using the usual performances index: SSE, STD and VarU criteria, which informs about the control effort of each controller Each index is averaged over the scenarios of operation and the global comparison is presented into an histogram in Fig. 6. This histogram is found representative of all scenarios of table 1, even when different blockage ratios were set (scenario 2 and 3). Scenario 2 has been arbitrarily selected in the rest of the analysis to illustrate the averaged performance of figure 6. Figures 7, 8, 9, 10 and 11, illustrate the tracking of the

300 instantaneous lift for each MFC, AST, PID(a), PID(b) and PID(c) controller, according to the evolution of the corresponding duty-cycle.

The model-free based approaches require very few information about the dynamical system to control. In particular, the lack of information about the system uses learning properties or adaptive properties of such controller that has to "guess" the behavior of the system. The AST offers globally better performances over all scenarios than MFC controller due to adaptive

305 integrator and adaptive gains associated to a sliding mode controller, that smooth the response according to high frequency variations of the lift dynamics. The performances are however very similar in Sc. #2 depicted in Fig. 7 and 8. On the other hand, the MFC contains an anticipating action (via numerical derivation) instead of the adaptive action, which makes this controller more reactive to small aerodynamic perturbations.

The comparison of the tracking between the three PID controllers shows that the particular controller, associated to the

310 polytope (c), shows a good tracking of the lift in the case of the perturbed wind flow including a inflow velocity change, meaning that this particular polytopic model matches the best the overall dynamics, whereas the other polytope based controllers give worse performances. Despite the strong difficulty to model the dynamic of the lift, one can assume that a very particular choice of the operating conditions to build the polytopic model could give interesting results. Note that the identification process to tune the robust PID control is difficult to maintain rigorous operating conditions in the wind tunnel considering this additional
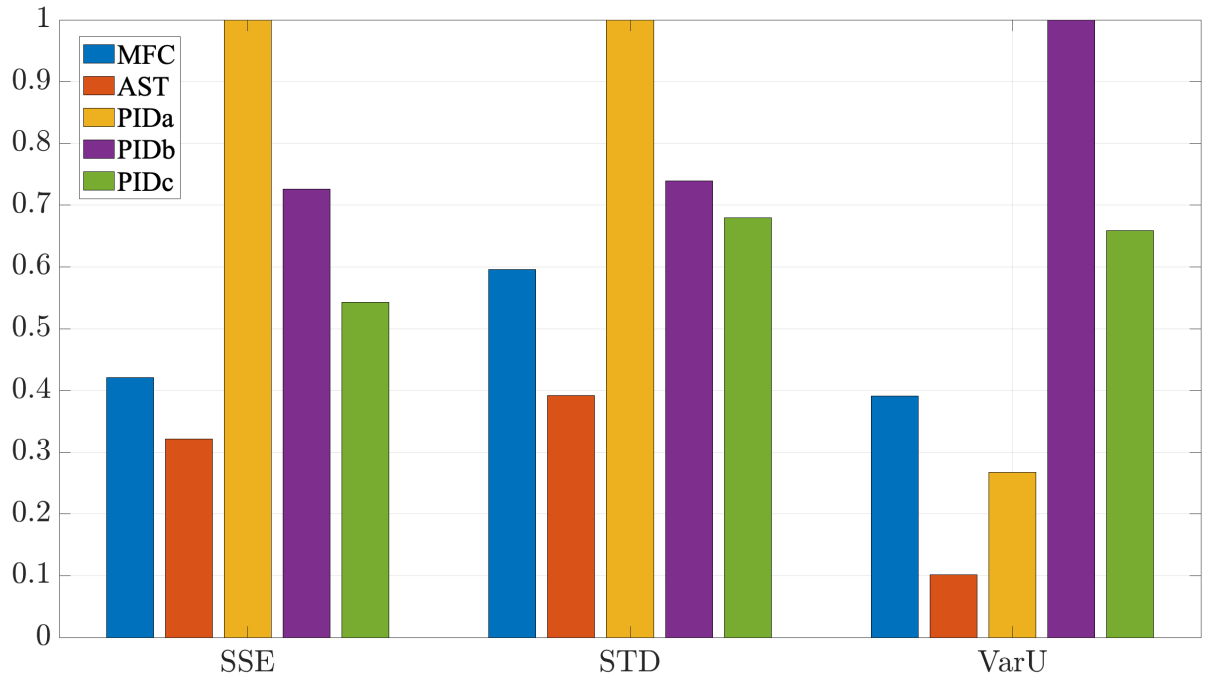
Figure 6. Normalized performances SSE, STD and VarU of the control laws (PID, MFC and AST) averaged over scenarios for each controller.

315 turbulence generated by the presence of the chopper. The identification has been performed by averaging several step responses of the measured lift. It is assumed that the dynamics of the micro-jet action is very fast, compared to the dynamics of the wind flow, to consider such averaged approximation. We yet notice *a posteriori* that the identification assumptions that the models depend of operating conditions and not on the average duty-cycle (the effective actuation force) seems erroneous: this reflects very different dynamics depending on the value of the reference lift, for which a closer identification would improve the models.

320   Focusing on the static response of each controller around 15 sec, Figs. 12 and 13 highlight the behavior of each controller for the Sc. #2 and #5 respectively. In both cases, MFC and AST show smooth responses than PID controllers. The responses of the PID controllers remain harmonic, inducing a worse rejection of the aerodynamic perturbation. Globally, the nonlinear properties of AST and MFC allow a better reduction of the aerodynamic perturbations whereas PID control is limited to rejects disturbances and tends to amplify oscillations (Fig. 12). Nevertheless, if the perturbation, induced by the chopper and variations

325 of the mean inflow velocity, increases, the rejection becomes less efficient for the nonlinear control AST and MFC (Fig. 13) but remains better than PID. Moreover, as observed previously in Sc. #2, Fig. 9, 10 and 11 highlight differences of the tracking efficiency according the level of the lift reference, hence, showing the limitation of the considered robust PID control.

Remark that in Fig. 8, the time needed for the AST controller to converge to the reference is slower due to the adaptation of the gains; this convergence issue is not general and depends strongly on the operation conditions. Due to the internal anticipation of the MFC structure, Fig. 7 shows good convergence to the reference, which is very similar to the behavior of the PID controllers.
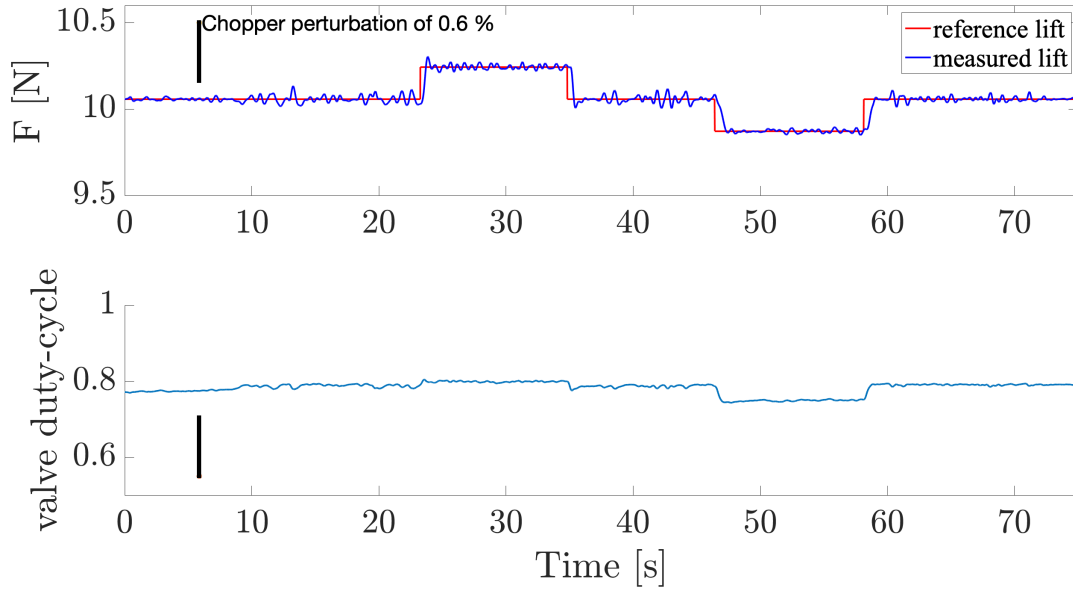
Figure 7. Time Evolution of the lift controlled by the MFC with respect to the lift reference (Top) and associated duty-cycle (Bottom). The chopper introduction is marked by the black vertical line.
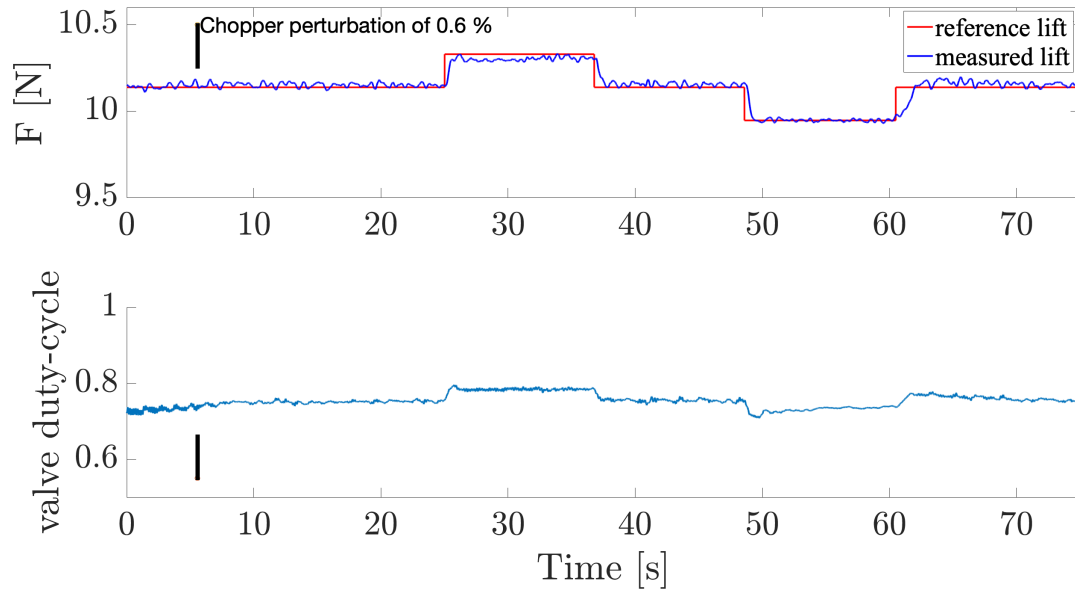
Figure 8. Time Evolution of the lift controlled by the AST with respect to the lift reference (Top) and associated duty-cycle (Bottom). The chopper introduction is marked by the black vertical line.
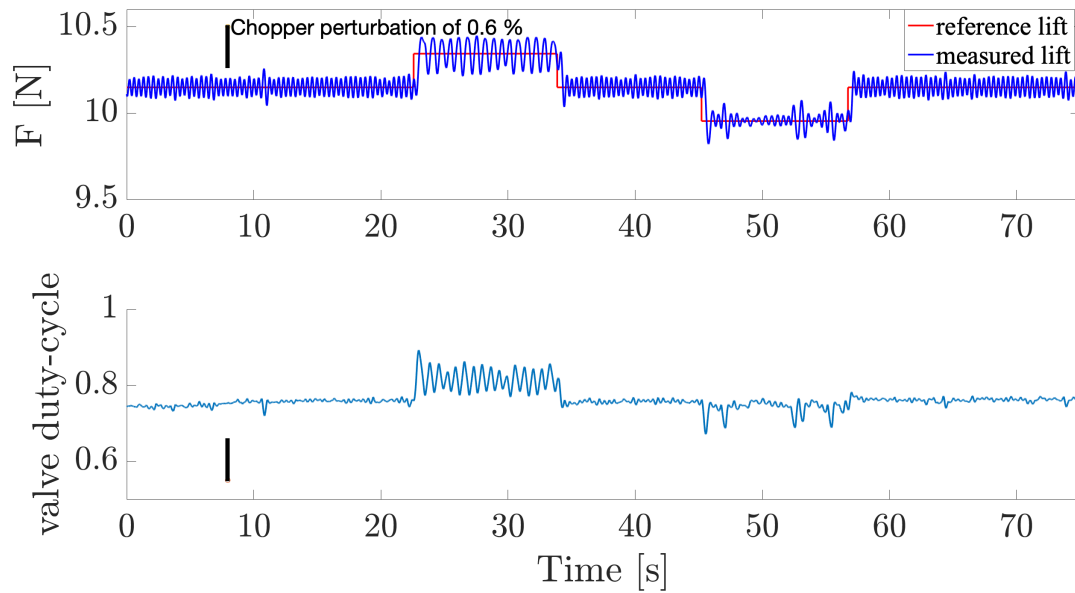
Figure 9. Time Evolution of the lift controlled by the PID(a) with respect to the lift reference (Top) and associated duty-cycle (Bottom). The chopper introduction is marked by the black vertical line.
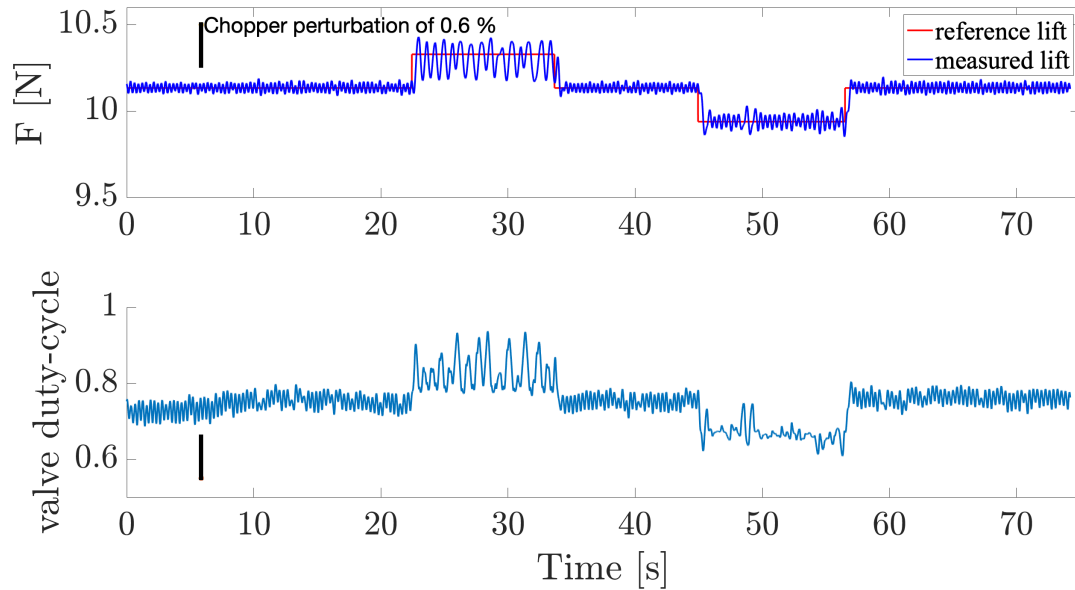
Figure 10. Time Evolution of the lift controlled by the PID(b) with respect to the lift reference (Top) and associated duty-cycle (Bottom). The chopper introduction is marked by the black vertical line.
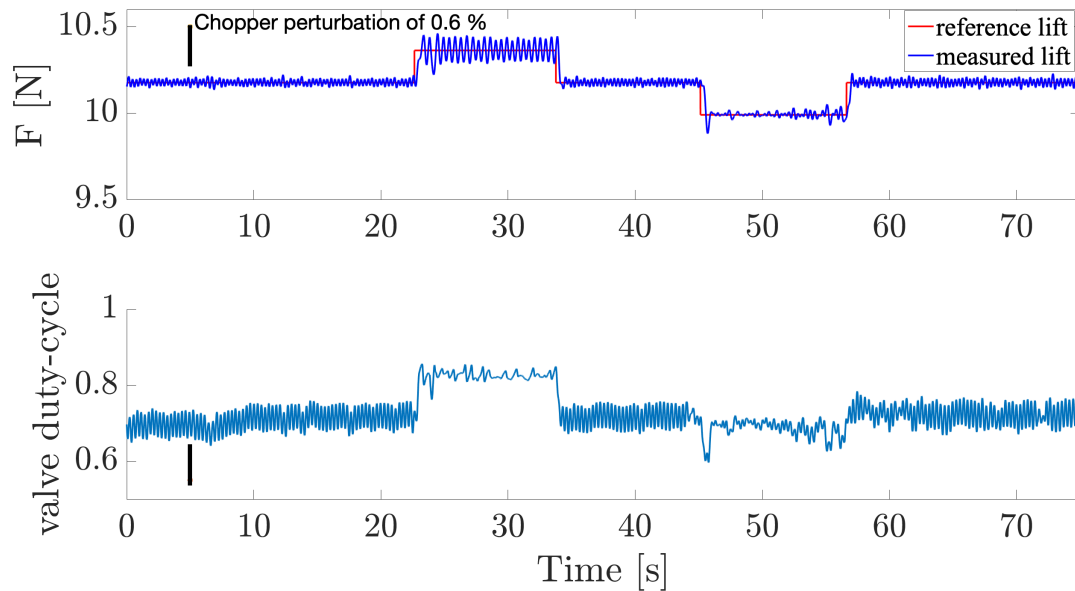
Figure 11. Time Evolution of the lift controlled by the PID(c) with respect to the lift reference (Top) and associated duty-cycle (Bottom). The chopper introduction is marked by the black vertical line.
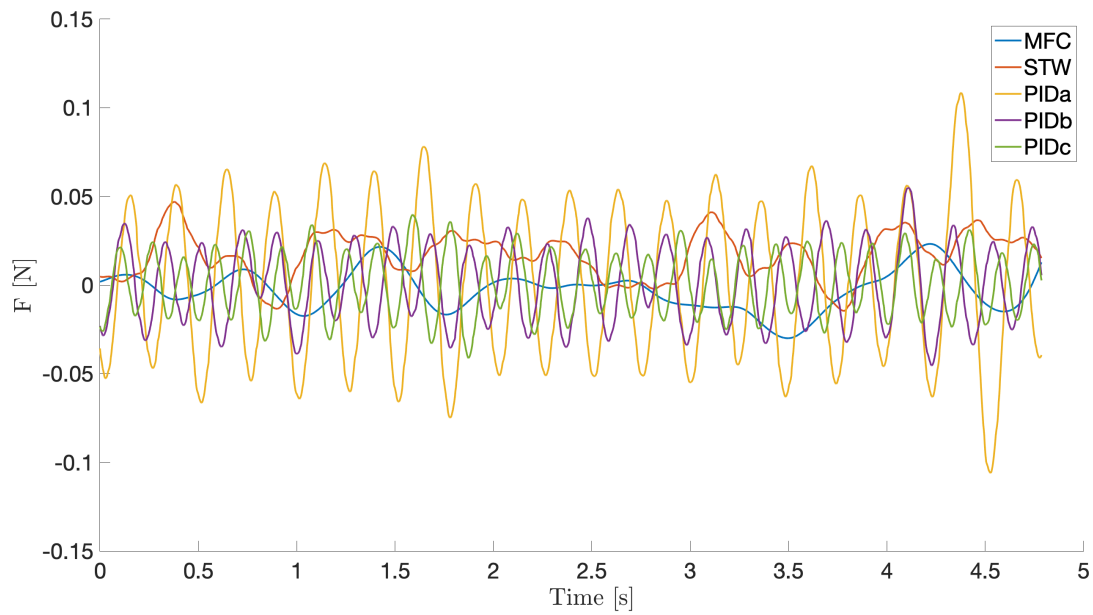
Figure 12. Starting sequence of Scenario #2 (see table 1): comparison of the Time evolution of the lift with each controller (PID, AST and MFC) for a constant inflow of 20 m.s^{-1} and no perturbation from the chopper system.
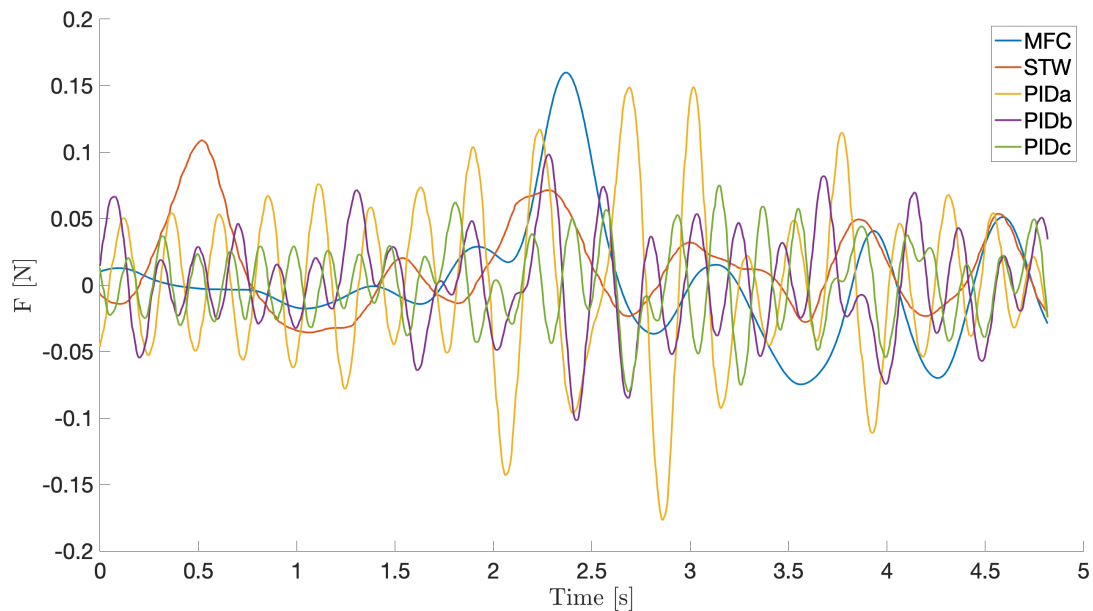
Figure 13. Starting sequence of Scenario #5 (see table 1): comparison of the time evolution of the lift with each controller (PID, AST and MFC) for a constant inflow of 20 m.s^{-1} and no perturbation from the chopper system.

Regarding the MFC and AST, these strategies are based on a very minimal knowledge of the system dynamic under study:
like the sign of the global transfer and the relative degree (the number of times that the input of the system is derived in order
to obtain the output); the sampling period is also of importance since it imposes limitations of the range of the gains. From the
gained experience, a rough tuning of the parameters gives already correct performances. Better performances could be obtained
by using an online optimization procedure that aims for example to minimize the Sum of Square Error of the controlled lift
over several portions of time. Nevertheless, this approach has not been envisaged in this paper because in limited available
time of the wind tunnel, it requires deeper developments to include an optimization algorithm to the embedded control and
measurements take time.

4.4.2 Analysis of performances in case of control saturation

The problem of saturation comes from the presence of integrator inside the controllers, hence introducing an anti-windup
algorithm to prevent the integrators from diverging (that induces in this case a saturation of the output y). As the MFC controller
does not contain a numerical integrator, the problem of the desaturation using an AW algorithm concerns only the AST and
PID controllers.

In the case of the Scenario #2, Figs 14, 15, 16 and 17, illustrate the tracking of the instantaneous lift for respectively the AST, PID(a), PID(b) and PID(c) controllers during the saturation mode, involving the Anti-Windup (AW) algorithm, at the beginning of the control operation.

355   The easiest AW algorithm is typically applied for the PID control (see e.g. Franklin et al. (1994), chap. 9 of the sixth edition), for which a single integrator needs to be frozen when saturation occurs. At the opposite, the more complex one is the AST, for which it is required to freeze four integrators (v, μ, k_1 and k_2) using a particular sequencing with respect to the gains management, which makes the tuning of its AW more difficult. The desaturation depends mainly on the integrators and gains, hence, the AST desaturation is slower. This is due to the time needed to re-adapt the gains (in the considered PID, the gains are

360   fixed). Remark that in Fig. 14, the behavior until 10 sec corresponds to the initialization sequence of k_1 and k_2 integrators. In order to highlight the initial adaptive time, both gains are initialized at very small values.
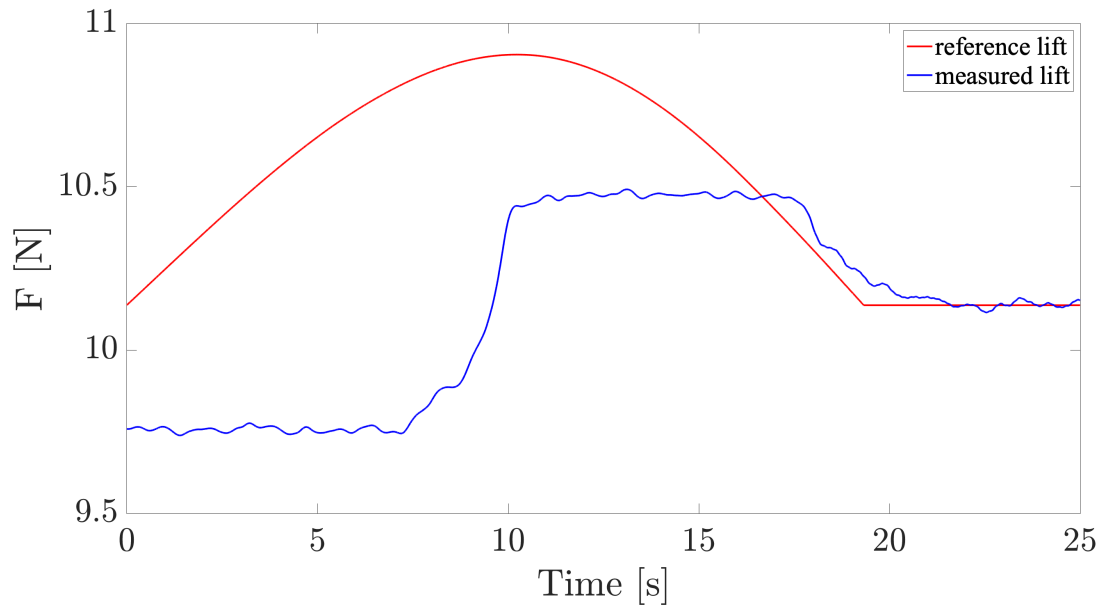
Figure 14. Saturation test: time evolution of the lift controlled by the AST algorithm under saturation (in blue) with respect to the lift reference (in red).

365

5   Conclusions

This work provides comprehensive knowledge from the gained experience about the practical design and implementation of some feedback control laws that succeed in performing aerodynamic lift control with active flow actuators. The investigations lead us to conceive an appropriate test-bench focusing on the lift control problem. Three control strategies have been selected, the parameters of the controllers were designed and implementation has been carried out on the test-bench. In summary the conclusions for each control are the following. The model-based strategy for the design of robust PID control has the advantage of being rather systematic but is highly dependent on prior model identification. As it assumes linear representation of the plant it is expected to perform mainly when the system is close to the set point. The two other control strategies are model-free (or assuming basic properties on the plant) but require hand tuning which may not be systematic. It revealed to be rather simple in the MFC case, and did not need *a posteriori* to build some Anti-Windup strategy to cope with saturation issues. The features of the adaptive super-twisting control revealed rather smooth time-responses. Comparing all tuned controllers in terms of close-loop performances but also the design and development time, MFC appears as a good compromise in case of saturation while AST provides slightly smoother responses. We are conscious that the conclusions in terms of performances may differ when applying other values on the control parameters. We claim not that the values are unique nor optimal. It may well be that the hierarchy of results changes for other versions of these same controls. One of the perspectives for the Automatic Control
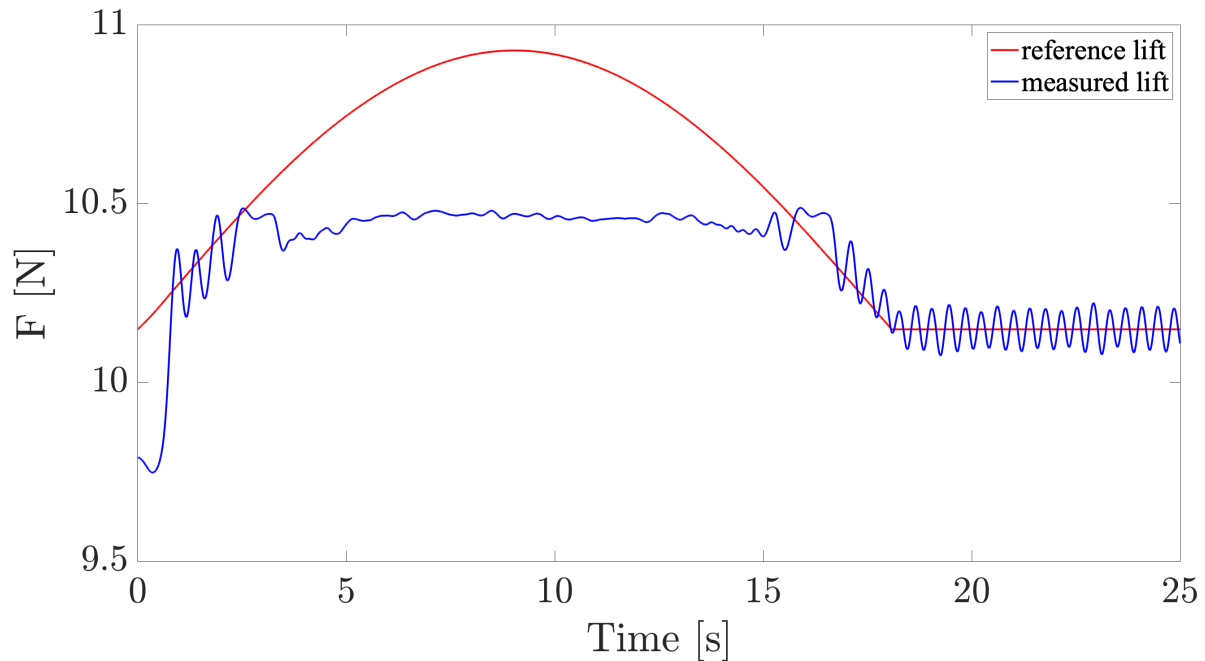
Figure 15. Saturation test: time evolution of the lift controlled by the PID(a) algorithm under saturation (in blue) with respect to the lift reference (in red).
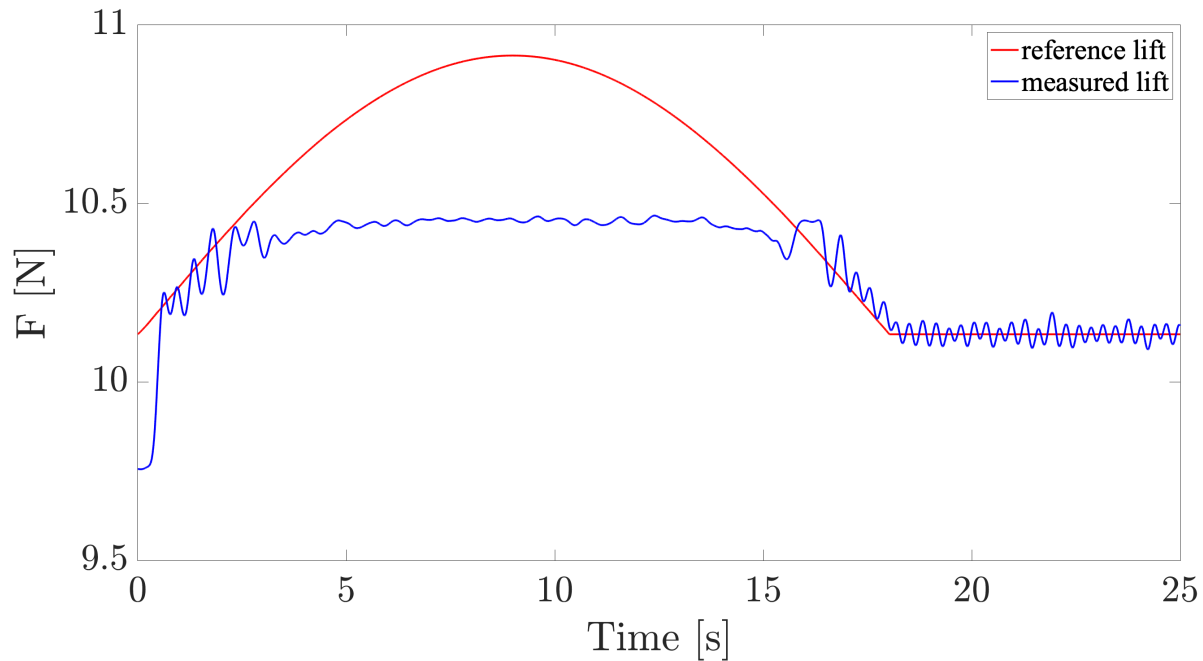
Figure 16. Saturation test: time evolution of the lift controlled by the PID(b) algorithm under saturation (in blue) with respect to the lift reference (in red).

colleagues involved in the project, is to establish mathematical tools to tune control parameters such that the controllers, at least locally, provide similar results. But this is out of the scope of the present work.

Code and data availability. All data (dataset and Matlab scripts to plot all figures) are available on this repository: https://zenodo.org/doi/10.5281/zenodo.10617750.

385 *Author contributions.* L. Michel carried out the conceptualization, the methodology, investigations, the software design and the preparation of the full paper. C. Braud, J.-P. Barbot and F. Plestan carried out the conceptualization, the methodology, investigations and the preparation of the full paper. In addition, C. Braud provided the experimental resssources and C. Braud and F. Plestan provided the funding acquisition. D. Peaucelle provided knowledge about robust PID design tools as well as a ready to use code for designing the control gains for given polytopes, and participated to the review of the paper. X. Boucher participated to the software design and the writing of the paper.

390 *Competing interests.* The authors declare that they have no conflict of interest.

Acknowledgements. The authors thank Michel Fliess and Cédric Join for they fruitful advices with respect to the model-free control algorithm implementation, which has been the starting point of our previous investigations of this study. The authors thank Dr. Pierre Molinaro for the design of the electronic control board in the experimental setup. This work was partially supported by ANR (*Agence Nationale de la Recherche*) with project CREATIF ANR-20-CE05-0039, by WEAMEC (West Atlantic Marine Energy Community) cluster with the projects ASAPe and FOWTBLADE, and by the Carnot GOWIBA project, funded by the Carnot Institute Marine Engineering Research for "Sustainable, Safe and Smart Seas". Jean-Pierre Barbot is supported with (*Région Pays de la Loire*) Connect Talent GENYDROGENE project.

395
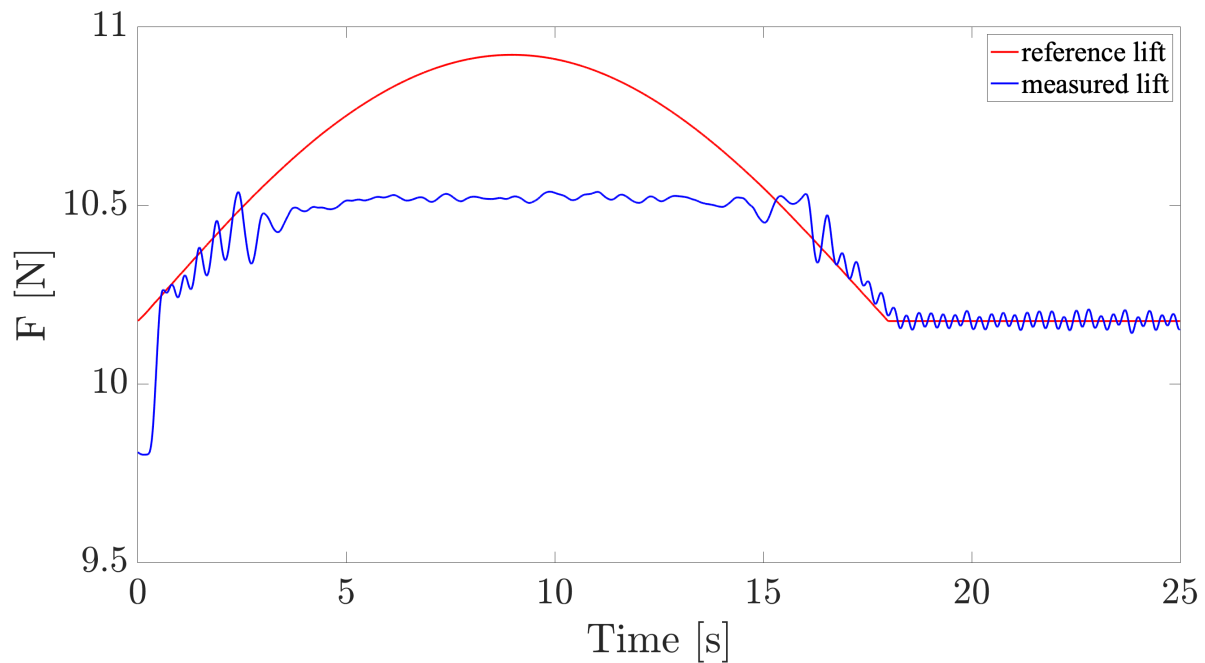
Figure 17. Saturation test: time evolution of the lift controlled by the PID(c) algorithm under saturation (in blue) with respect to the lift reference (in red).

References

Albertos, P. and Sala, A.: Iterative Identification and Control: Advances in Theory and Applications, ISBN 978-1-4471-1098-9, https://doi.org/10.1007/978-1-4471-0205-2, 2002.

Allan, B. G., Juang, J., Raney, D. L., Seifert, A., Pack, L. G., and Brown, D. E.: Closed-loop Separation Control Using Oscillatory Flow Excitation, Tech. rep., NASA/CR-2000-210324, ICASE Report 2000-32, 2000.

Aubrun, S., Leroy, A., and Devinant, P.: A review of wind turbine-oriented active flow control strategies, Experiments in Fluids, 58, https://doi.org/10.1007/s00348-017-2412-0, 2017.

Barlas, T., van Wingerden, J. W., Hulskamp, A., and van Kuik, G.: Closed-Loop Control Wind Tunnel Tests on an Adaptive Wind Turbine Blade for Load Reduction, in: 46th AIAA Aerospace Sciences Meeting and Exhibit, https://doi.org/10.2514/6.2008-1318, 2008.

Bartholomay, S. et al.: Pressure-based lift estimation and its application to feedforward load control employing trailing-edge flaps, Wind Energy Science, 6, 221–245, https://doi.org/10.5194/wes-6-221-2021, 2021.

Becker, R., Garwon, M., Gutknecht, C., Barwolf, G., and King, R.: Robust control of separated shear flows in simulation and experiment, J. of Process Control, 15, 691–700, 2005.

Becker, R., King, R., Petz, R., and Nitsche, W.: Adative Closed-loop separation control on a high-lift configuration using extremum seeking, AIAA Journal, 45, 1382–1392, 2007.

Bossanyi, E.: The Design of Closed Loop Controllers for Wind Turbines, Wind Energy, 3, 149–163, 2000.

Braud, C., Podvin, B., and Deparday, J.: Study of the wall pressure variations on the stall inception of a thick cambered profile at high Reynolds number, Phys. Rev. Fluids, 9, 014 605, https://doi.org/10.1103/PhysRevFluids.9.014605, 2024.

Brunner, C. E., Kiefer, J., Hansen, M. O. L., and Hultmark, M.: Study of Reynolds number effects on the aerodynamics of a moderately thick airfoil using a high-pressure wind tunnel, Experiments in Fluids, 62, 2021.

Brunton, S. and Rowley, C.: Low-Dimensional State-Space Representations for Classical Unsteady Aerodynamic Models, https://doi.org/10.2514/6.2011-476, 2010.

Conord, T. and Peaucelle, D.: Multi-Performance State-Feedback for Time-Varying Linear Systems, in: Third IFAC Conference on Modelling, Identification and Control of Nonlinear Systems - MICNON 2021, Online, Japan, https://hal.laas.fr/hal-03176042, 2021.

Fliess, M. and Join, C.: Model-free control, International Journal of Control, 86, 2228–2252, 2013.

Fliess, M. and Join, C.: An alternative to proportional-integral and proportional-integral-derivative regulators: Intelligent proportional-derivative regulators, Int J Robust Nonlinear Control, pp. 1–13, 2021.

Franklin, G., Powell, J., and Emami-Naeini, A.: Feedback Control Of Dynamic Systems, 1994.

Gault, D. E.: A correlation of low-speed airfoil-section stalling characteristics with Reynolds number and airfoil geometry, Tech. Rep. Technical note 3963, National Advisory Committee for Aeronautics, 1957.

Isidori, A.: Nonlinear control systems: an introduction, Springer, 1985.

Jaunet, V. and Braud, C.: Experiments on lift dynamics and feedback control of a wind turbine blade section, Renewable Energy, 126, 65–78, 2018.

Lafont, F., Balmat, J.-F., Join, C., and Flieś, M.: First steps toward a simple but efficient model-free control synthesis for variable-speed wind turbines, International Journal of Circuits, Systems and Signal Processing, 14, 1181–1191, 2020.

Li, N. and Balas, M. J.: Adaptive Flow Control of Wind Turbine Blade Using Microtabs with Unsteady Aerodynamic Loads, in: 2013 IEEE Green Technologies Conference (GreenTech), pp. 134–139, 2013.

435 McCullough, G. B. and Gault, D. E.: Example of three representative types of airfoil-section stall at low speed, Technical Note NACA TN 2502, National Advisory Committee for Aeronautics, Moffett Field, California, United States, 1951.

Michel, L., Selvarajan, S., Ghanes, M., Plestan, F., Aoustin, Y., and Barbot, J.-P.: An Experimental Investigation of Discretized Homogeneous Differentiators: Pneumatic Actuator Case, IEEE Journal of Emerging and Selected Topics in Industrial Electronics, 2, 227–236, https://doi.org/10.1109/JESTIE.2021.3061924, 2021.

440 Michel, L., Neunaber, I., Mishra, R., Braud, C., Plestan, F., Barbot, J.-P., Boucher, X., Join, C., and Fliess, M.: Model-free control of the dynamic lift of a wind turbine blade section: experimental results, Journal of Physics: Conference Series, 2265, 032 068, https://doi.org/10.1088/1742-6596/2265/3/032068, 2022.

Michel, L., Neunaber, I., Mishra, R., Braud, C., Plestan, F., Barbot, J.-P., and Hamon, P.: A Novel Lift Controller for a Wind Turbine Blade Section Using an Active Flow Control Device Including Saturations: Experimental Results, IEEE Transactions on Control Systems

445 Technology, pp. 1–12, https://doi.org/10.1109/TCST.2023.3345208, 2024.

Mirzaei, M. J., Hamida, M. A., Plestan, F., and Taleb, M.: Super-twisting sliding mode controller with self-tuning adaptive gains, European Journal of Control, 68, 100 690, https://doi.org/https://doi.org/10.1016/j.ejcon.2022.100690, 2022 European Control Conference Special Issue, 2022.

Mojallizadeh, M. R., Brogliato, B., Polyakov, A., Selvarajan, S., Michel, L., Plestan, F., Ghanes, M., Barbot, J.-P., and Aoustin, Y.: A survey

450 on the discrete-time differentiators in closed-loop control systems: Experiments on an electro-pneumatic system, Control Engineering Practice, 136, 105 546, https://doi.org/https://doi.org/10.1016/j.conengprac.2023.105546, 2023.

Neunaber, I. and Braud, C.: First characterization of a new perturbation system for gust generation: the chopper, Wind Energy Science, 5, 759–773, 2020.

Park, B., Zhang, Y., Olama, M., and Kuruganti, T.: Model-free control for frequency response support in microgrids utilizing wind turbines,

455 Electric Power Systems Research, 194, 107 080, 2021.

Peaucelle, D., Tremba, A., Arzelier, D., Bortott, A., Calafiore, G., Chevarria, G., Dabbene, F., Polyak, B., Shcherbakov, P., Sevin, M., Spiesser, P., and Tempo, R.: R-RoMulOC: Randomized and Robust Multi-Objective Control toolbox, http://projects.laas.fr/OLOCEP/romuloc, 2014.

Peaucelle, D., Guilmineau, E., and Braud, C.: Towards robust control design for active flow control on wind turbine blades, in: Wind Energy

460 Science Conference 2019, p. paper id 706, Cork, Ireland, https://hal.science/hal-02888544, 2019.

Plestan, F. and Taleb, M.: Adaptive supertwisting controller with reduced set of parameters, in: 2021 European Control Conference (ECC), pp. 2627–2632, 2021.

Rezaeiha, A., Pereira, R., and Kotsonis, M.: Fluctuations of angle of attack and lift coefficient and the resultant fatigue loads for a large Horizontal Axis Wind turbine, Renewable Energy, 114, 904–916, https://doi.org/https://doi.org/10.1016/j.renene.2017.07.101, 2017.

465 Scheinker, A.: 100 years of extremum seeking: A survey, Automatica, 161, 111 481, https://doi.org/https://doi.org/10.1016/j.automatica.2023.111481, 2024.

Schepers, J., Boorsma, K., Madsen, H., Pirrung, G., Bangga, G., Guma, G., Lutz, T., Potentier, T., Braud, C., Guilmineau, E., Croce, A., Cacciola, S., Schaffarczyk, A. P., Lobo, B. A., Ivanell, S., Asmuth, H., Bertagnolio, F., Sørensen, N., Shen, W. Z., Grinderslev, C., Forsting, A. M., Blondel, F., Bozonnet, P., Boisard, R., Yassin, K., Hoening, L., Stoevesandt, B., Imiela, M., Greco, L., Testa, C., Magionesi, F.,

470 Vijayakumar, G., Ananthan, S., Sprague, M. A., Branlard, E., Jonkman, J., Carrion, M., Parkinson, S., and Cicirello, E.: IEA Wind TCP Task 29, Phase IV: Detailed Aerodynamics of Wind Turbines, https://doi.org/10.5281/zenodo.4813068, 2021.

Shtessel, Y., Plestan, F., Edwards, C., and Levant, A.: Adaptive Sliding Mode and Higher Order Sliding-Mode Control Techniques with Applications: A Survey, pp. 267–305, Springer International Publishing, Cham, 2023.

Soulier, A., Braud, C., Voisin, D., and Podvin, B.: Low-Reynolds-number investigations on the ability of the strip of Tell-Tale sensor to detect flow features over wind turbine blades: flow separation/reattachment dynamics, Wind Energy Science, 6, 409–426, 2021.

Tarbouriech, S., Garcia, G., Silva, J., and Queinnec, I.: Stability and Stabilization of Linear Systems with Saturating Actuators, ISBN 978-0-85729-940-6, https://doi.org/10.1007/978-0-85729-941-3, 2011.

Wagner, S., Bareiß, R., and Guidati, G.: Wind Turbine Noise, 1996.

Williams, D. R. and King, R.: Alleviating Unsteady Aerodynamic Loads with Closed-Loop Flow Control, AIAA Journal, 56, 2194–2207, https://doi.org/10.2514/1.J056817, 2018.

Åström, K. J. and Murray, R. M.: Feedback Systems, Princeton University Press, 2008.